



# Sound intensity-based panel noise contribution analysis for improving the acoustic performance of a vehicle interior

E. Güven<sup>1</sup>, D. Fernandez-Comesaña<sup>2</sup> and T. Marini Storani<sup>3</sup>

<sup>1</sup>Hyundai Motor Europe Technical Center GmbH, Email: egueven@hyundai-europe.com

<sup>2</sup>Microflown Technologies B.V., Email: fernandez@microflown.com

<sup>3</sup>Microflown Technologies B.V., Email: storani@microflown.com

## Abstract

One of the main NVH goals of most car manufacturers is to enhance acoustic performance while meeting demanding weight and cost targets. Typical vehicle optimization strategies are designed via numerical simulations and later adjusted through modal and noise testing. Although traditional techniques are reasonably effective, they are often very laborious and time-consuming. This paper proposes a novel methodology to identify key radiation areas and rank their importance towards the front and rear passengers. An extension of the substitution monopole technique is introduced, combining 3D sound intensity measurements and acoustic transfer functions. The suggested measurement approach significantly simplifies the refinement process of a vehicle interior, reducing the traditional testing process to just a few days. Details about the measurement methodology are presented in this paper along with a vehicle investigation performed on a roller test bench for several operational conditions. The experimental results demonstrated that the proposed technique provides an extensive amount of vibro-acoustic data for every vehicle section, including noise ranking and visualization of complex acoustic phenomena in three-dimensional space. This information was successfully used for designing and improving the acoustic package of a commercial electric vehicle.

## Introduction

The vibro-acoustic properties of a car cabin play a key role in the perception of vehicle quality. All vehicles include an acoustic package comprising various components such as absorbers, barriers, dampers, and isolators which aim to improve the noise performance [1]. Increasing pressure from weight and emissions targets means that automotive OEMs are being challenged to meet customer expectations for NVH performance in ever more efficient ways and, of course, without inflating the cost of production.

The rapid development in computational processing power has enabled the use of numerical simulations to determine the dynamic response of complex structures with reasonable accuracy [2]-[6]. These techniques are effective especially in the early stages of the design cycle. However, substantial discrepancies are often found between simulations and experiments which led to the development of hybrid techniques [7] or purely experimental methods [8].

Traditionally, experimental techniques are used to optimize the size and location of damping treatments. In particular, laser vibrometer-type tests are often conducted on body-in-white structures enabling the fast acquisition of a large number of measurement points with a good spatial resolution. However, testing a complete vehicle is mostly unfeasible, requiring an independent evaluation of each subsystem, hence limiting the usability of this technology.

Scanning-based measurement methodologies have been proven suitable for performing noise localization in a fast and efficient way [9]. However, there are still difficulties to overcome when using this type of data for source ranking, especially in complex environments such as a vehicle interior. The main purpose of this study is to introduce a measurement methodology for designing an effective acoustic treatment of a vehicle using scanning 3D sound intensity measurements. Sound intensity

measurements are combined with static acoustic transfer functions to evaluate the importance of multiple problematic areas towards a set of reference positions. The fundamental theory about both sound intensity and panel noise contribution analysis is hereby covered. Furthermore, several experimental examples are evaluated with the proposed methodology, including a full-vehicle validation.

## Sound intensity

Sound intensity is a measure of the flow of acoustic energy in a sound field [10]. It provides not only a quantification of the acoustic emission but also the direction of sound propagation, since it is a vector quantity. The instantaneous sound intensity is defined as the product of sound pressure and acoustic particle velocity

$$\mathbf{I}(t) = p(t)\mathbf{u}(t). \quad (1)$$

[W/m<sup>2</sup>]

Sound pressure and acoustic particle velocity have level and phase differences which mainly depend upon the characteristic of the sound source, measurement distance and frequency [11]. In practice it is common to study stationary sound fields in terms of the active, or propagating, part of the complex intensity averaged over time [12], i.e.

$$\mathbf{I} = [I_x, I_y, I_z] = \langle p \mathbf{u} \rangle_t = \frac{1}{2} \operatorname{Re}\{p \mathbf{u}^*\}, \quad (2)$$

[W/m<sup>2</sup>]

where  $\langle \cdot \rangle_t$  indicates time averaging. The imaginary part of this quantity is known as the reactive intensity  $J$ , which represents the non-propagating acoustic energy. Unlike the usual active intensity, the reactive intensity remains to some extend controversial probably because it has no obvious physical meaning [10]. Experimental evidence is presented in the following sections for both active and reactive intensity, discussing the practical significance of both quantities.

Figure 1 shows schematic representations of the 3D active intensity vector and the one-dimensional (1D) complex acoustic intensity, where  $\theta_p - \theta_{u_n}$  represents the phase difference between the sound pressure and a particle velocity component.

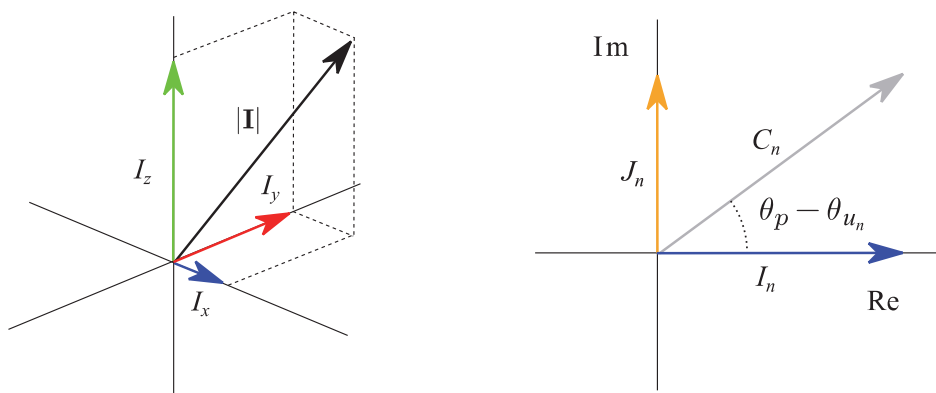


**Figure 1:** Schematic representation of the 3D active intensity vector (left) and 1D complex acoustic intensity (right).

Since both sound pressure and particle velocity are measured simultaneously, the calculation of the 3D acoustic intensity can be performed directly, without any approximation. This quantity provides directional information about the flow of acoustic energy. In addition, a scalar term can be extracted by taking the modulus of the active intensity vector.



Extensive research has been published exploring the fundamental differences between multiple sound intensity measurement principles and transducers [13]. Pressure-based measurement methods cannot be utilized when the pressure-intensity index is high, which in practice often limits the use of p-p intensity probes in environments with high background noise or reflections. A detailed analysis of this phenomenon is described in [14].

In contrast, direct intensity measurements using the combination of sound pressure and particle velocity transducers (p-u intensity probes) are unaffected by the pressure-intensity index, enabling the estimation of propagating acoustic energy despite unfavorable conditions imposed by the testing environment. The error of intensity calculations using p-u probes mainly depends upon the reactivity of the sound field and the calibration accuracy of the probe [13]

$$\hat{I}_n \cong I_n \left( 1 + \varphi_u \frac{J_n}{I_n} \right) = I_n \left( 1 + b\{\hat{I}_n\} \right), \quad [\text{W/m}^2] \quad (3)$$

where  $\varphi_u$  is the phase error introduced during the calibration procedure,  $J_n$  is the reactive intensity and  $b\{\cdot\}$  denotes the bias error of an estimate. If the reactivity is high, for example in the near field of a source, a small phase mismatch in the transducer's calibration may lead to considerable errors on the intensity estimates. Although active intensity may be biased in a highly reactive field, the phase difference between pressure and particle velocity can still be measured accurately. Therefore, it is still possible to discard measurement positions that are exposed to high reactivity and ensure that the most reliable data is evaluated.

## Fundamentals of Panel Noise Contribution Analysis

This section considers the theoretical framework for deriving the fundamentals of PNCA. The following derivation follows Williams [15], although the same expression can also be obtained from the principle of reciprocity, as shown by J.Hald [16].

The sound pressure  $p_{\text{ref}}$  located at the reference position  $\mathbf{x}$  due to a continuous radiating surface  $S$  can be derived from the Kirchhoff-Helmholtz Integral Equation using Green's functions

$$p_{\text{ref}}(\mathbf{x}) = \int_S \left( G(\mathbf{x}, \mathbf{y}) \frac{\partial p(\mathbf{y})}{\partial n} - p(\mathbf{y}) \frac{\partial G(\mathbf{x}, \mathbf{y})}{\partial n} \right) dS, \quad [\text{Pa}] \quad (4)$$

where  $p(\mathbf{y})$  is the sound pressure at position  $\mathbf{y}$  on the surface  $S$ ,  $\partial/\partial n$  denotes normal derivative on the surface and  $G(\mathbf{x}, \mathbf{y})$  is the Green function that relates the propagation between the points  $\mathbf{x}$  and  $\mathbf{y}$ . Under free-field conditions, Green's function can be determined via analytical solutions. However, most practical scenarios contain elements that affect sound propagation between the assessed points. Alternatively, Green functions can also be acquired experimentally by measuring the acoustic pressure perceived at a point  $\mathbf{x}$  in response to a monopole sound source of controlled source acceleration  $j\omega\rho Q$  located at  $\mathbf{y}$ , therefore [10]

$$G(\mathbf{x}, \mathbf{y}) = \frac{p^{\text{TF}}(\mathbf{x})}{j\omega\rho Q(\mathbf{y})}, \quad [m^{-1}] \quad (5)$$

where  $Q(\mathbf{y})$  is the volume velocity of the monopole sound source,  $\omega$  is the angular frequency,  $\rho$  is the density of air and  $p^{\text{TF}}(\mathbf{x})$  is the sound pressure measured when a monopole source is exciting the sound field. It should be noted that Eq. 2 implies that a monopole source needs to be positioned at every measurement location  $\mathbf{y}$ . A reciprocal measurement is often easier to perform. According to the reciprocity theorem, source and receiver can be interchanged, i.e.  $G(\mathbf{x}, \mathbf{y}) = G(\mathbf{y}, \mathbf{x})$ , as long as the spatial domain can be considered time-invariant. As a result, the experimental characterization of the Green functions is often performed by placing a monopole source at the reference position  $\mathbf{x}$  while

measuring near the radiating surface  $\mathbf{y}$ . Furthermore, Euler's equation of motion makes it possible to obtain an expression for the spatial derivative of the measured Green's function given in Eq. 1 as such

$$\frac{\partial G(\mathbf{y}, \mathbf{x})}{\partial n} = \frac{\partial p^{\text{TF}}(\mathbf{y})/\partial n}{j\omega\rho Q(\mathbf{x})} = \frac{u_n^{\text{TF}}(\mathbf{y})}{Q(\mathbf{x})}, \quad [m^{-2}] \quad (6)$$

where  $u_n^{\text{TF}}(\mathbf{y})$  represents the acoustic particle velocity measured normal to the surface  $S$  when exciting the sound field with a monopole source located at the reference position. The combination of Eq. 1, Eq. 2 and Eq. 3 yields

$$p_{\text{ref}}(\mathbf{x}) = \int_S \left( \frac{p^{\text{TF}}(\mathbf{y})}{Q(\mathbf{x})} u_n(\mathbf{y}) - p(\mathbf{y}) \frac{u_n^{\text{TF}}(\mathbf{y})}{Q(\mathbf{x})} \right) dS. \quad [\text{Pa}] \quad (7)$$

It can be shown that the second term of the integral vanishes when data is acquired directly at a rigid boundary [17]. Such an approximation, often referred to as the hard-wall assumption, is used by most pressure-based panel contribution methods.

For the practical implementation of Eq. 4 it is necessary to subdivide the surface  $S$  into  $N$  small sections of area  $\Delta S_i$ . Consequently, Eq. 4 can be written in a discrete form as

$$p_{\text{ref}}(\mathbf{x}) \approx \sum_{i=1}^N \left( \frac{p^{\text{TF}}(\mathbf{y}_i)}{Q(\mathbf{x})} u_n(\mathbf{y}_i) \right) \Delta S_i. \quad [\text{Pa}] \quad (8)$$

The above expression enables the reconstruction of the sound pressure  $p_{\text{ref}}$  at a reference position  $\mathbf{x}$  by measuring the sound field at  $N$  measurement points. When assessing the noise radiated by a complex structure, such as a vehicle cabin interior, it is convenient to study the contribution of the different constructive elements using several measurement positions. This implies that  $K$  probes are grouped in order to calculate the partial contribution of each element. A similar expression can be derived following the substitution monopole technique theory, where each panel energy is defined by their locally measured sound power, i.e.

$$|p_{\text{ref}}(\mathbf{x})|^2 \approx \sum_{i=1}^N \left| \left( \frac{\kappa_0}{\omega} \frac{p^{\text{TF}}(\mathbf{y}_i)}{Q(\mathbf{x})} \sqrt{W(\mathbf{y}_i)} \right) \right|^2. \quad [\text{Pa}] \quad (9)$$

where  $\kappa_0$  is a weighting factor common for all panels. The proposed expression combines sound intensity information together reciprocally measured acoustic transfer functions, therefore being suitable with scanning methods.

## Measurement method: Scan&Paint 3D

The sound visualization system used to capture the information hereby presented was Scan&Paint 3D [18]. The system comprises the following hardware elements:

- 3D tracker: automatic real-time 3D tracking of the sensor position and orientation using a stereo infrared camera.
- Data acquisition unit: 24 bit, 4 channel data acquisition system.
- Signal conditioner: signal conditioning unit for supplying power and pre-amplification to the 3D sound intensity probe.
- 3D sound intensity probe: broadband 3D intensity probe (20 Hz to 10 kHz) consisting of a sound pressure microphone and 3 acoustic particle velocity sensors.
- Tracking sphere: open sphere with scattered IR reflecting markers for tracking the probe location and orientation.



- Remote handle: control and monitor the data acquisition process.

Before measuring the acoustic field it is required to have a 3D model of the testing object. The model can be either imported from a CAD file or obtained by scanning the area of interest with a structural scanner. Results presented below were acquired using a 3D scanner known as a structure sensor [19]. The model is used as a visual reference as well as to automatically position the 3D tracker into the measuring environment. The acoustic data acquisition process starts by manually moving a 3D sound intensity probe whilst a stereo camera is used to extract the instantaneous position of the sensor in the 3D space.

The recorded signals are split into multiple segments and assigned to their corresponding locations using a spatial discretization algorithm [18]. The spatial resolution is defined during the post-processing stage and thus can be adjusted depending on the available data. The maximum feasible resolution is determined by the accuracy of the 3D tracker, in this case, down to 3 millimeters.

A particle velocity or sound intensity vector representation of the acoustic variations across the sound field can then be computed to provide a visual representation of the sound distribution. Figure 2 shows the main hardware elements, experimental setup, and analysis software.

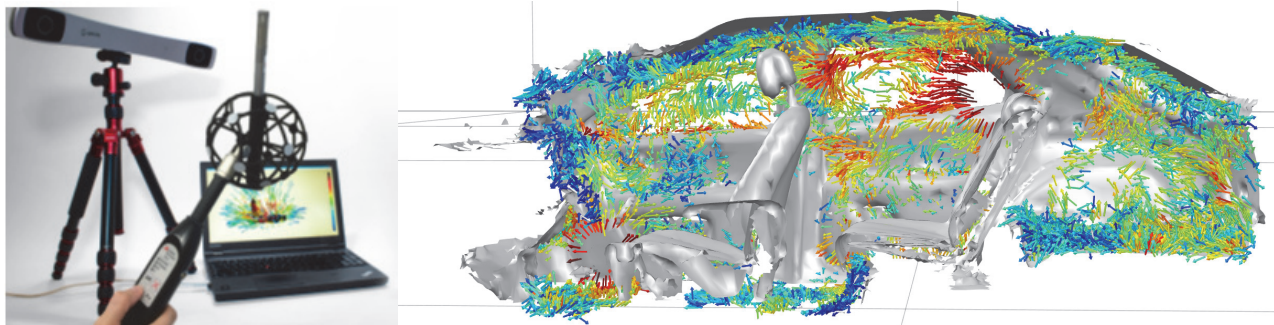


**Figure 2:** Figure 2. Scan&Paint 3D hardware (left) and example result of the sound intensity field measured inside a vehicle interior (right).

## Experimental investigation

The measurement campaign evaluated in this study focuses on evaluating the noise produced by an electric car while running on a dyno inside a semi-anechoic chamber at 80 KPH and 100 KPH. Operational experiments were carried at the testing facilities of SEGULA Technologies GmbH, whereas the transfer functions were measured at HMETC (Rüsselsheim am Main, DE).



**Figure 3:** Figure 3. on semi-anechoic vehicle dyno constant speed measurement at 80kph and 100kph (left) and example of the sound intensity field measurement inside of vehicle (right).

## Scanning measurements

Multiple measurements were performed around a car interior at two operational regimes (80 KPH and 100 KPH), aiming to achieve high spatial resolution sound mapping. A 3D sound intensity probe was manually moved close to all car surfaces, scanning the entire vehicle for each operational condition independently. For both car speeds 80 scans were performed. 2 reference microphones were used at the front and rear of the cabin during scans. The average scanning time was about 100 seconds per scan. The total time was of 2 days, including setup, camera repositioning, troubleshooting the dyno, and data acquisition. The recorded data were segmented using a 15 mm spatial resolution grid, yielding more than 16000 data points. A picture of the setup is shown in Figure 4, along with a preview of the scanned structure highlighting the scanning traces with different colors.



**Figure 4:** Scanning traces of the entire measurement campaign.

## 3D sound intensity visualization

The large dataset acquired contains information about the spatial distribution of sound pressure, particle velocity, and (active & reactive) sound intensity inside the entire vehicle in full 3D space. Sound visualization results with a spatial resolution of 15 mm are displayed in Figure 5:. As shown, the two critical bands evaluated have very different behavior. For lower frequencies, the trunk has the highest acoustic emission, whereas the C pillar, B pillar, and rear passenger windows seem to dominate the medium frequency range. Therefore, demonstrating how the sound intensity is much larger when measured close to the emitting panels. For lower frequencies, the trunk has the highest acoustic emission, whereas the C pillar, B pillar, and rear passenger windows seem to dominate the medium frequency range.

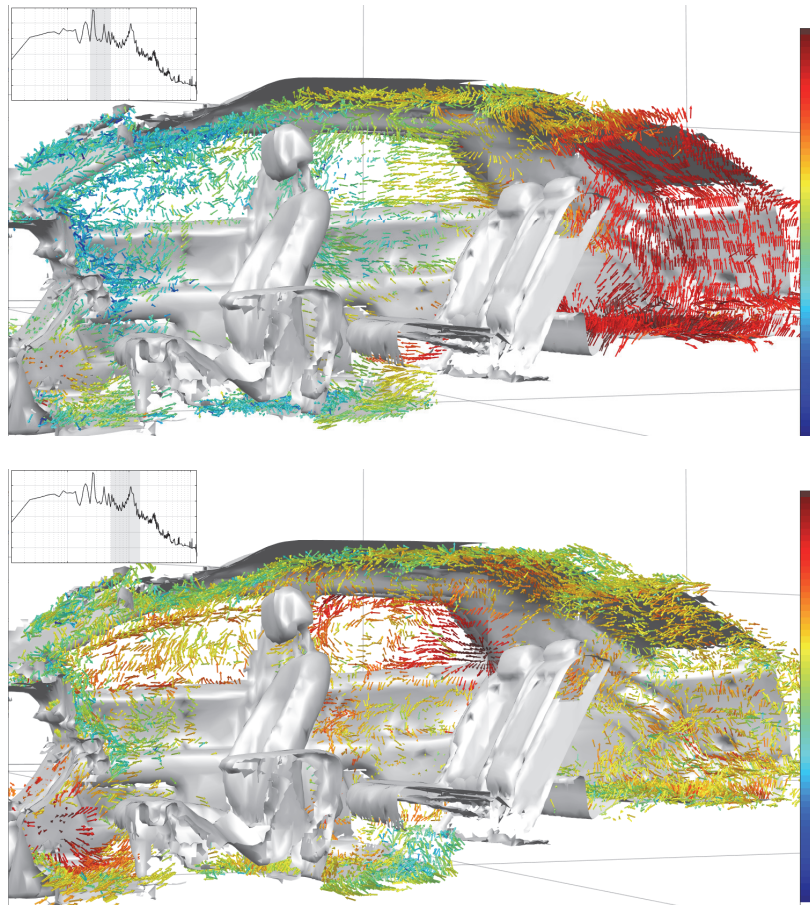


**Figure 5:** 3D Sound intensity maps measure at 80 KPH at two critical frequency bands.

## Acoustic Transfer Functions

Reciprocal transfer functions were measured using 2 Microflown Volume Velocity Sources (Low Frequency and Mid-High Frequency) at a series of discrete locations. 78 points were measured for 5 seconds using white noise excitation with each source individually and for each reference position. A total of 312 measurements were performed. Each condition (78 points per source & reference) were tested in about 35 minutes. Total measuring time, including setup, data acquisition, and preparation was about 5 hours.

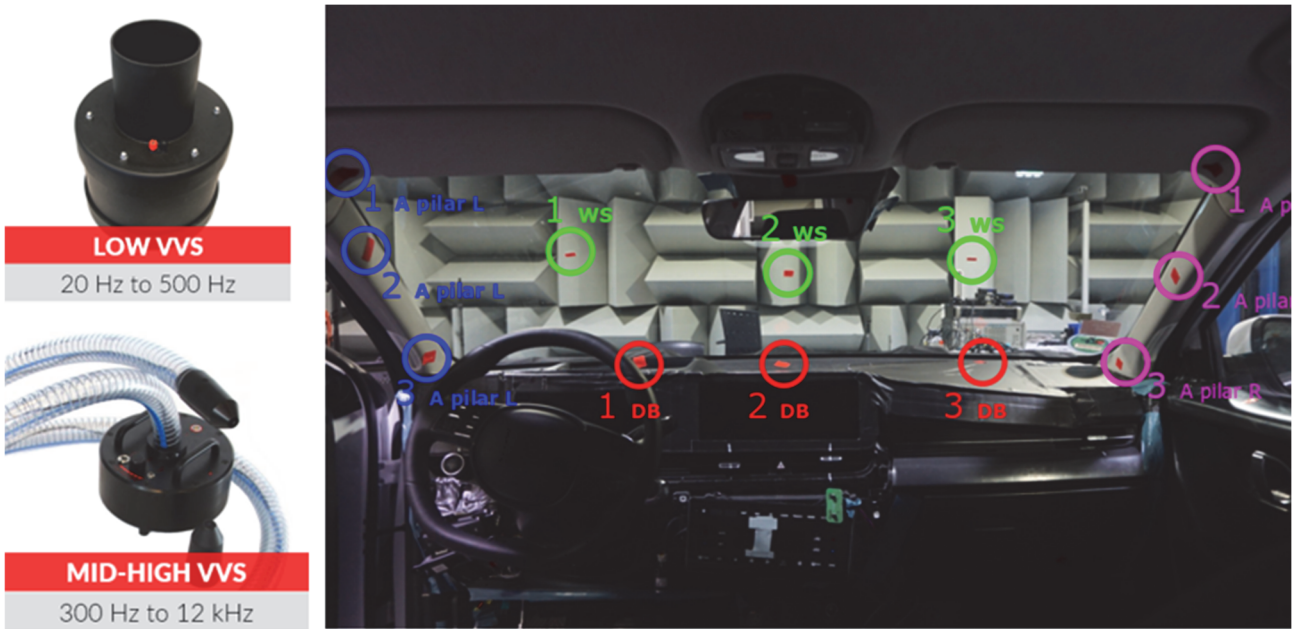


**Figure 6:** Low (top left) and mid-high (bottom left) volume velocity sources along with a picture of an example of the discrete points measured during the reciprocal transfer function testing.

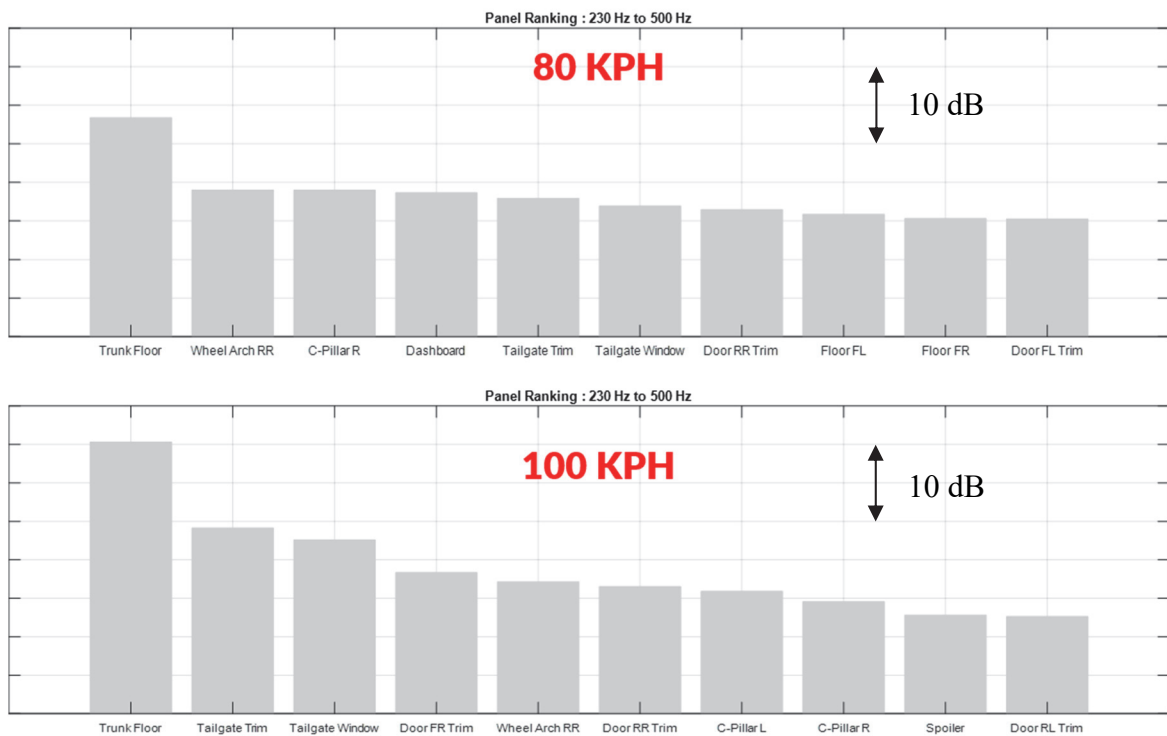


**Figure 7:** Source ranking of the main car sections focused on one problematic frequency range.

## Panel Ranking

Sound pressure contributions of different car sections were calculated by combining near-field sound intensity measurements with their corresponding sound propagation paths (Eq. 9). The entire vehicle was discretized in 30 panels related to the most relevant constructive elements, of which the sound intensity and acoustic transfer functions were spatially averaged. Figure 7: shows an example of the panel ranking analysis performed in each of the critical frequency bands for multiple operational



conditions. As shown, it is clear that the trunk floor was the dominant panel to improve in order to reduce the noise at this frequency band.

## Conclusions

A novel measurement methodology to perform high-resolution 3D sound visualization and panel noise contribution analysis was introduced. A practical case, a full car interior, has been evaluated using the presented measurement methodology. 3D sound intensity measurements acquired near the different car surfaces were proven to be useful to visualize the acoustic emission of different constructive elements. As shown, the visualization of sound intensity in a 3D space enables us to get an intuitive and comprehensive understanding of sound radiation mechanisms as well as the interaction between problematic elements. Finally, a ranking of the main sections of the car interior was presented, showing that the combination of reciprocally measured acoustic transfer functions with 3D sound intensity measurements can reveal the main problematic areas for multiple operational conditions and/or frequency bands. This information was used to apply an effective acoustic treatment in order to reduce the noise perceived by the vehicle's passengers.

## Literature

- [1] Subramanian, S., R. Surampudi, K. R. Thomson, and S. Vallurupalli. Optimization of damping treatment for structure borne noise reduction. No. 2003-01-1592. SAE Technical Paper, 2003.
- [2] Subramanian, S., R. Surampudi, K. R. Thomson, and S. Vallurupalli. "Optimization of Damping Treatments for Structure Borne Noise Reductions." *Sound and Vibration* 38, no. 9 (2004): 14-19.
- [3] Subic, A., A. Markowicz, and A. Bourmistrova. "Shape optimization of damping liners on vibrating panels." In *Proceedings of the International Congress on Modelling and Simulation-Advances and Applications for Management and Decision Making*. Modelling and Simulation Society of Australia and New Zealand. 2005.
- [4] Wang, Binxing, Sifa Zheng, Lin Zhou, Shengqiang Liu, Xiaomin Lian, and Keqiang Li. "Acoustic modelling and analysis of vehicle interior noise based on numerical calculation." In *Intelligent Computation Technology and Automation (ICICTA), 2010 International Conference on*, vol. 1, pp. 404-407. IEEE, 2010.
- [5] Zheng, Ling, Zhanpeng Fang, Zhongcai Tang, Zhenfei Zhan, and Jiang-hua Fu. The design optimization of vehicle interior noise through structural modification and constrained layer damping treatment. No. 2015-01-0663. SAE Technical Paper, 2015.
- [6] Georgiev, Vasil B., R. L. Ranavaya, and Victor V. Krylov. "Finite element and experimental modelling of structure-borne vehicle interior noise." *Noise Theory and Practice* 1, no. 2 (2015).
- [7] Siavoshani, Saeed, Jay Tudor, and Dev Barpanda. Vehicle body optimization of structural noise and vibration using a hybrid technique. No. 2007-01-2327. SAE Technical Paper, 2007.
- [8] Furukava, Márcio, Samir Gerges, Miguel M. Neves, and Bento JL Coelho. "Analysis of structural damping performance in passenger vehicles chassis." *J. Acoust. Soc. Am* 126 (2009): 22-80.
- [9] Fernandez Comesana, Daniel. "Scan-based sound visualisation methods using sound pressure and particle velocity." PhD Thesis, University of Southampton, 2014.
- [10] Jacobsen, F., and Juhl, P. M., "Fundamentals of general linear acoustics," John Wiley & Sons, 2013.
- [11] Kinsler, L.E., Frey, A.R., Coppens, A.B., Sanders J. V., "Fundamentals of acoustics," Wiley, 2000.
- [12] Fahy, F.J. "Sound Intensity," E&FN Spon, 2nd edition, 1995.
- [13] Jacobsen, F., and de Bree, H.-E., "A comparison of two different sound intensity measurement principles." *Journal of the Acoustical Society of America* 118(3): 1510-1517, 2005.
- [14] Jacobsen, F., and de Bree, H.-E.. "Measurement of sound intensity: p-u probes versus p-p probes," In proceedings of NOVEM, 2005.

- [15] E. G. Williams, "Fourier Acoustics: Sound Radiation and Nearfield Acoustical Holography," Academic Press, 1999.
- [16] J. Hald, M. Tsuchiya, C. Blaabjerg, H. Ando, T. Yamashita, M. Kimura and Y. Ishii, "Panel contribution analysis using a volume velocity source and a double layer array with the SONAH algorithm. In InterNoise and NoiseCon Congress and Conference Proceedings, vol. 2006, no. 6, pp. 1465-1474, Institute of Noise Control Engineering, 2006.
- [17] O. Wolff , "Fast panel noise contribution analysis using large PU sensor arrays," in Proceedings of Internoise, 2007.
- [18] Fernandez Comesaña, D., Steltenpool, S., Korbasiewicz, M., and Tijs, E., "Direct acoustic vector field mapping: new scanning tools for measuring 3D sound intensity in 3D space," In proceedings of Euronoise, pp. 891-895, 2015.
- [19] Occipital, Inc. "The structure sensor", <https://www.structure.io/>, 2008 (accessed 8th December 2019).